HHS Public Access

Author manuscript

Lab Chip. Author manuscript; available in PMC 2019 January 30.

Published in final edited form as:

Lab Chip. 2018 January 30; 18(3): 451–462. doi:10.1039/c7lc00724h.

Razor-printed sticker microdevices for cell-based applications

Loren E. Stallcop[1,*], **Yasmín R. Álvarez-García**[2,*], **Ana M. Reyes-Ramos**[3], **Karla P. Ramos-Cruz**[3], **Molly M. Morgan**[4], **Yatao Shi**[5], **Lingjun Li**[2,5], **David J. Beebe**[4,6], **Maribella Domenech**[3], and **Jay W. Warrick**[4]

[1]Univ. of Wisconsin - Madison, Dept. of Materials Science - Madison, WI, USA

[2]Univ. of Wisconsin - Madison, Dept. of Chemistry - Madison, WI, USA

[3]Univ. of Puerto Rico - Mayaguez, Dept. of Chemical Eng. - Mayaguez, PR

[4]Univ. of Wisconsin - Madison, Dept. of Biomedical Eng. - Madison, WI, USA

[5]Univ. of Wisconsin -Madison, School of Pharmacy - Madison, WI, USA

[6]Univ. of Wisconsin -Madison, Carbone Cancer Center - Madison, WI, USA

Abstract

Tape-based razor-printing is a flexible and affordable ultra-rapid prototyping approach for microscale device fabrication. However, integration of this prototyping approach into cell-based assay development has been limited to proof of principle demonstrations. This is in large part due to lack of an established or well-characterized option for biocompatible adhesive tape. Without such an option, integration of these areas will remain unexplored. Therefore, to address this critical hurdle, we characterized microscale devices made using a potentially biocompatible double-sided adhesive, ARCare 90106. We validated tape-based device performance against 96-well plates and PDMS microdevices with respect to cell viability, hydrophobic small molecule sequestration, the potential for leaching compounds, use in fluorescence microscopy, and outgassing (bubble formation). Results supported the tape as a promising tool for future cell-based assay development. Therefore, we subsequently demonstrated specific strengths enabled by the ultra-rapid (< 1hr per prototype) and affordable (~$1,200 cutting plotter, < $0.05 per prototype) approach. Specifically, data demonstrate the ability to integrate disparate materials for advanced sticker-device functionality such as bonding of polystyrene devices to glass substrates for microscopy applications, inclusion of membranes, and incorporation of different electrospun biomaterials into a single device. Likewise, the approach allowed rapid adoption by uninitiated users. Overall, this study provides a necessary and unique contribution to the largely separate fields of tape-based razor-printing and cell-based microscale assay development by addressing a critical barrier to widespread integration and adoption while also demonstrating the potential for new and future applications.

Correspondence to: Maribella Domenech; Jay W. Warrick.

*Contributed equally

Keywords

xurography; razor-printing; microscale cell culture; biocompatible double-sided pressure-sensitive adhesive; open microfluidics; patterned electrospun biomaterials

INTRODUCTION

Razor-printing (xurography) can be used as an ultra-rapid microscale fabrication method that is growing in popularity [1–11] and complements other microfabrication approaches such as soft-lithography, micromilling, laser-cutting, and 3D printing. [12–17] Razor-printing allows device components to be cut or “printed” from sheets of material (e.g., polymers and double-sided adhesive tapes) using a cutting plotter that is operationally similar to a standard home inkjet printer with X-Y resolutions as precise as 20 μm. [2,18–20] Given the similarity to ink-jet technology, cutting plotters are affordable and easy to use. A particular strength of razor-printing is the ability to leverage double-sided adhesive tapes to enable bonding of device components for layered fabrication of microdevices. [21–23] This approach is referred to here as tape-based razor-printing fabrication and enables bonding of disparate materials such as glass and plastic or integration of functional materials for advanced device functionality (e.g., membranes). Further, the resultant device can be thought of as a sticker that can be applied to a wide range of substrates for use in unique applications and contexts (e.g., skin using dermal adhesives). For these reasons, tape-based razor-printing provides an ultra-rapid, simple, affordable, and flexible platform for microscale device development.

Although the benefits of tape-based razor-printing microscale tool development have been recognized previously, use of the approach has generally been limited to biochemical applications and has not yet been an extensively demonstrated or characterized for cell-culture applications. Current efforts to apply razor-printing for cell-based applications have been limited to qualitative demonstrations of cells grown in razor-printed devices. [2,22,24] Indeed, application of this flexible, ultra-rapid prototyping approach in cell-based assays will remain limited without tested or validated options for biocompatible adhesive tapes. If this hurdle is addressed, tape-based razor-printing has the potential to significantly impact microscale tool development for cell-based applications by enabling 1) integration of disparate materials for advanced functionality; 2) rapid adoption and innovation by a broader user community; and 3) new applications via the ‘sticker-like’ properties of the devices.

To help address this critical hurdle we identified and performed characterization and validation of a biocompatible double-sided adhesive tape (ARcare 90106, Adhesives Research, Glen Rock, PA), subsequently referred to here as ‘Tape’. We chose Tape because it was used successfully in previous cell-based assays; [2,22,24] however, as with other potential tape options, validation against analogous devices without tape was lacking. Suitability for cell culture with multiple cell lines was demonstrated using a simple and flexible open microfluidic co-culture device design to complement the simple and rapid fabrication approach. [25–27] Validation was performed by comparing to culture in 96-well plates and analogous devices made from PDMS, the gold standard microscale culture device material. Additional characteristics important for microscale culture applications were also

characterized, such as outgassing (bubble formation), absorption of lipophilic molecules, the potential for compounds to leach from the tape into aqueous media during culture, as well as the cost and time for prototyping and fabrication. Results represent, to our knowledge, a first comparative biological validation of taped-based razor-printing for cell-based applications. Upon validation, we then demonstrated how the tape enables rapid prototyping of cell culture assay designs, integration of disparate materials for advanced sticker-like device functionality, and rapid adoption by uninitiated undergraduate users. Thus, although the experiments described here integrate existing technologies, they represent a new and critical scientific contribution that is needed to significantly advance the use of powerful tape-based razor-printing fabrication methods in cell-based microscale assay development.

EXPERIMENTAL

Fabrication methods

Razor-printing (Xurography) was performed with a Graphtec Craft ROBO Pro, CE5000-40-CRP cutting plotter (Graphtec America, Irvine, CA, USA) equipped with a 0.9 mm diameter and 60° angle Graphtec blade (CB09UA). According to the manufacturer, the purchased Tape (ARCare 90106) consists of a clear polyester substrate coated on both sides with MA-69 acrylic hybrid medical grade adhesive. Tape (without protective backing on both sides) has a total thickness of 143 ± 14.3 μm. Polystyrene (PS) (Goodfellow, ST313300, 0.05 mm thick) and Tape can be obtained directly as sheets or rolls for razor-printing, whereas sheets of PDMS were made (see Device Assembly C). Designs were drawn and cut using Adobe Illustrator (AI) and the free Graphtec plugin for AI, Cutting Master 3. *Soft lithography*[16,17] was used to mold devices from polydimethylsiloxane (PDMS, Sylgard 184 silicone elastomer kit, Dow Corning, Auburn, MI) for comparison with razor-printing. *Micromilling* was performed using Solidworks (Dassault Systems, France) and a CNC mill (Tormach, pCNC 700) to design and cut devices as described previously. [13] Briefly, devices were cut from 2 mm thick PS sheets, sonicated and soaked in 100% isopropyl alcohol, then rinsed with DI water to remove potential contaminants such as milling lubricants.

Device assembly

All devices were placed in plasma-treated (Femto, Diener, Thierry Corporation, Royal Oak, MI) 50 mm glass bottom Petri dishes (MatTek Corporation, Ashland, MA) and subsequently UV sterilized for consistency between experimental conditions. *A. Soft lithography (*Fig 2A) - PDMS devices made via soft lithography were first placed in 95% ethanol for 12–24 hrs to remove uncrosslinked oligomers, a process referred to as ethanol extraction. [28] Extracted devices were then dried and plasma bonded to the glass-bottom culture dishes. [17] *B. Milled PS + Tape (*Fig 2B) - Clean micromilled devices were adhered to plasma treated 50 mm glass bottom Petri dishes using Tape. Tape was cut with the protective backings in place. Once cut, one side of the backing was removed for placing the tape onto the micromilled PS. The tape was aligned to the PS device using a milled PS template with alignment posts that co-register holes in the tape with holes in the PS, enabling alignment of features to ~ ± 50 μm. Finally, the last layer of backing was removed to place the PS device in the glass bottom culture dish. *C. PDMS razor-printing (*Fig 2C) - Sheets of PDMS were made by razor-printing a Tape gasket or spacer that is placed between transparency sheets to mold sheets of

PDMS (cured at 80 °C for 3.5 hours). Device layers were then cut from the sheets, ethanol extracted, dried, and layered in plasma treated culture dishes to create multi-level laminated devices. *D. PS-Tape razor-printing (*Fig 2D) - A PS sheet was first wiped with 100% isopropanol, then applied to one surface of Tape with a soft rubber brayer. This PS-Tape laminate was then taped down to a sheet of transparency at its edges and fed through the cutting plotter to cut device layers. The layers were washed with soap (Alconox, Fisher Scientific, 16-000-108) and water, thoroughly rinsed with water and blown dry. Layers can then be placed down in sequence to build a multi-layer device on the glass bottom culture dish.

Device design and operation

An “open” microscale co-culture device design consisting of multiple adjacent culture regions within a larger parent well is used throughout the majority of experiments for consistent comparison and analysis (Fig 1E). Different cell populations can be seeded into each small culture region, while a fluid overlay retained by the parent well can be used to allow soluble factor signaling between each culture well. The culture regions have a diameter of 2.7 mm while the parent well containing the culture regions has a diameter of 8 mm. The culture regions and parent well have different heights depending upon the method of fabrication (Fig 2), yet the volumes applied to each are held consistent throughout. To operate the devices, 8.5 μL of cell suspension at 400,000 cells/mL was loaded into culture regions. Cells were allowed to settle to the bottom of the culture regions for one hour at 37°C before being overlaid with 15 μL of warm media. Allowing the cells to settle to the bottom before overlaying was crucial to avoid mixing of cells between culture wells. For non-adherent cell types (e.g., RPMI 8226), gentle pipetting from the edges of the parent well is used to avoid transfer of cells between adjacent culture regions. In order to minimize evaporation and increase humidity of the devices, 150 μL of water and PBS was placed around the inside edge of the Petri dish. Petri dishes were also placed within bioassay dishes containing 50:50 PBS:water during incubation.

Cell culture and endpoints

Cell culture—MDA-MB-468, MDA-MB-231, HS578T, and NIH-3T3 were purchased from American Tissue Culture Collection (ATCC). The immortalized human mammary fibroblasts (HMFs) used here were derived from a reduction mammoplasty [29] and donated by Dr. Lisa Arndt’s lab (University of Wisconsin, Madison). These cell lines were maintained in complete cell culture medium consisting of DMEM high glucose media with L-Glutamine (100-017-CV, Corning), supplemented with 10% heat inactivated fetal bovine serum (16140071, Gibco), 1% amphotericin B (SV3007801, Fisher Scientific), and 1% penicillin/streptomycin (30001Cl, Corning) and maintained at 37°C in a 5% CO_2 incubator. Cells were passaged with a 0.05% Trypsin–EDTA solution (25300062, ThermoFisher) when near 75–80% confluence. Viable cells were counted based on Trypan Blue exclusion (T8154, Sigma-Aldrich) using a hemocytometer, diluted to the desired cell densities, and seeded in culture wells.

MCF-7 (mammary gland breast epithelial cells), LNCaP (prostate epithelial cells), and RPMI 8226 (human multiple myeloma cells) were cultured in RPMI 1640 media

(22400-105, Gibco) with 10% FBS fetal bovine serum, 1% penicillin streptomycin P/S (15140-122, Gibco), 2% Glutamax (35050-061, Gibco) and cultured at 37°C with 5% CO_2. Adherent cells were passaged with 0.05% Trypsin-EDTA (25300062, ThermoFisher). Cells were passaged every 2 to 3 days or when near 75–80% confluence.

Cell viability experiments (Fig 3A)—Cell viability analysis was performed using calcein AM (C3100MP, Life Technologies) and ethidium homodimer (EtHD, L3224, Life Technologies) at 24 hours post-seeding. The log of the ratio of the calcein and EtHD signals were quantified from microscopy images using JEX. [30] Expectation maximization clustering was performed on the log ratio data to identify 2 clusters, LIVE and DEAD. The % cell viability is calculated as LIVE / (LIVE + DEAD).

Estradiol dose-response (Fig 3C)—MVLN ERE luciferase reporter cells [31] were cultured in PS-Tape and PDMS nested co-culture devices. The luciferase expression (E1601, Promega) was measured while still in the cells using a BioRad ChemiDoc MP Imager and analyzed in the equipment software (Image Lab). The zero treatment control was subtracted from each biological replicate and normalized to the max of that replicate. The mean across replicates was then determined and normalized once again to the fit curve to a range of 0% to 100% activation. Curve fitting was performed with the 'drc' package in R to determine EC50 parameters and model standard errors.

AldeRed ALDH assay (Fig 3D)—MDA-MB-231 and MDA-MB-468 monocultures were seeded at a cell density of 5,000 cells/culture area in 96-well plates and the nested co-culture device made of PDMS or razor-cut PS. Cells were cultured in DMEM HG + L-glutamine + 0.5% FBS + 1% pen/strep or DMEM HG without phenol red + L-glutamine + 10% charcoal-stripped FBS +1% pen/strep for 96 hrs in a humidified incubator 5% CO_2 at 37°C. After 96 hrs, cells were removed from culture by washing once with PBS, incubating with 0.5% trypsin-EDTA for 2 min at 37°C, and re-suspending in cell culture medium for evaluation using the AldeRed Assay (SCR150, Millipore). A total of 6 microwells were collected into a single microcentrifuge tube to measure fluorescence intensity in the Cellometer (CBA Vision Nexcelom Cellometer).

Cell morphology analysis (Fig 3E & 3F)—Analysis was performed with JEX [32], an open-source, platform independent java-based software developed by the authors that leverages the image processing libraries of ImageJ [33] and ImageJ2 [34] to automate objective batch image processing. Briefly, a variance filter (radius 2 pixels) was applied to brightfield images to enable thresholding regions of cell cytoplasm. Nuclear images were background subtracted and thresholded to identify nuclei. Thresholded images of the cytoplasm (gray) and nuclei (blue) were then overlaid to visualize cell morphology. For each field of view, average area per cell = total cytoplasmic area / number of nuclei. Equivalent average cell radius is calculated as sqrt(average area per cell / π).

Immunostaining (Fig 4B)—Devices with cultured cells were fixed in 4% (vol/vol) paraformaldehyde (30525-89-4, Alfa Aesar) for 15 min and washed 3x with 1X PBS for 10 min at room temperature. Cells were permeabilized with 0.2% (vol/vol) Triton-X (807423, MP Biomedicals) in 1X PBS for 30 min at room temperature, washed 3x with 1X PBS for

10 min, and blocked with 3% (wt/vol) BSA (A9056, Sigma-Aldrich) in 1X PBS overnight at 4°C. Devices were then incubated in Alexa Fluor® 647 anti-human CD326 (EpCAM) Antibody (324212, BioLegend) diluted 1:50 and DAPI (D3571, Thermo) in 3% BSA at 4°C overnight before being washed with 1X PBS. Images were taken at 30x on a Nikon Eclipse Ti (Melville, NY) microscope equipped with a Hamamatsu Orca-Flash4.0 camera and SPECTRA X light engine (Lumencore, Beaverton, OR).

MALDI-ToF MS (Fig S1)—1.5mg 2-(4-hydroxyphenylazo) benzoic acid (HABA) (Sigma-Aldrich, CAS# 1634-82-8) was dissolved into 1 mL ACN/H_2O (50%/50%, V/V) as the matrix solution. To each of the dried samples stored in glass bottles, 20μl ethanol was added and mixed well. 1μL sample solution was mixed with 1μL matrix solution, which was further deposited onto a MTP 384 target plate (Bruker, part no. 209520) and rapidly air-dried for MALDI-MS analysis. Sample analysis was performed on an ultrafleXtreme MALDI ToF/ToF mass spectrometer (Bruker Daltonics, Germany) in a positive ion mode with laser energy of 60% and mass range of 1000–5000 Da. Data of each sample was acquired by accumulating four spectra at four different positions with 5000 laser shots per position. Positive controls (100% ethanol incubated with tape to dissolve tape components) and negative controls (matrix only) were compared to water samples incubated in 2.7 mm open wells (PS-Tape laminate on glass). Prior to placing the PS-Tape laminate device on a glass substrate, the laminate was washed either 0, 5, 10, or 20 washes with DI H_2O. Each wash was performed by putting the tape into a 50 mL polypropylene tube, filling the tube with fresh DI-H_2O, shaking for 30 s, and removing the fluid. Water samples (5μL) from 70 different open wells were aggregated, lyophilized, and resuspended in 10 μL of ethanol, to significantly concentrate (35-fold) compounds released into the aqueous solution. Comparison of the positive and negative controls identified a range of m/z ratios where a gaussian distribution of peaks characteristic of polymer molecules could be detected. The gaussian region was then exported and plotted using R for comparison.

RESULTS

Cell-culture viability

To demonstrate and compare the suitability of tape-based razor-printed devices for cell-based assays, we compared monoculture of 3 different well-studied cell lines (LNCaP, MCF-7, and RPMI 8226) in 4 different device constructions (Fig 2, A-D) with that of monoculture in a 96-well plate. Culture results of the different construction methods are shown in Fig 3. We observed that 2D culture in the microfabricated devices exhibited cell viabilities specific to each cell type and were similar to the viabilities seen in 96-well plate culture (Fig 3A). When the viability data for each cell type is normalized to its 96-well plate viability to pool data across cell types; fabrication methods A, B, and C had normalized viabilities of 98 ± 3 %, 99 ± 1 %, and 97 ± 4%, respectively. Thus, monoculture viability in the nested co-culture devices, regardless of fabrication method and presence or absence of tape, was nearly identical to monoculture culture in 96-well plates.

Cost, time, and resolution comparison of device construction methods

To aid comparison of razor-printed device fabrication with other approaches, Tab 1 is used to summarize the speed, precision, and affordability of the different construction methods used in Fig 2 and 3.

Absorption of small hydrophobic molecules

Given the hydrophobicity of ARcare 90106, we assessed the potential for small hydrophobic molecules (e.g., estrogens) to be sequestered into the polymer bulk as is seen with PDMS.[28,35] Fig 3B qualitatively illustrates the absorption/adsorption of nile red, a small fluorescent lipophilic molecule, for a PDMS and PS-Tape device. Interaction with the nile red is limited to the exposed edges of the tape given it is largely covered by PS whereas the PDMS device can absorb the nile red across wherever it contacts the nile red solution (e.g., between wells). Despite different fluorescence patterns, the dose-response of MVLN ERE luciferase reporter cells to estradiol (E2) did not show a significant difference in the EC50 parameter (Fig 3C, $p=0.78$) and was similar to previously reported data for these cells in traditional culture plates (33 pM).[36]

To further investigate whether the tape was absorbing hydrophobic small molecules, we used an AldeRed assay to quantify ALDH1, a positive marker of cancer stem-cell-like cells within tumor cell populations (Fig 3D). Another breast cancer cell line, MDA-MB-231, was included to further corroborate results. The percent of ALDH1^{HI} cells was ~ 5 fold higher in PDMS devices compared to both PS devices and a 96 well-plate ($p < 0.05$). PS-Tape and 96-well plate results were very similar, showing no significant difference for each cell line ($p > 0.6$). Thus, PDMS appeared to increase the putative cancer-stem-cell-like fraction relative to PS-Tape and 96-well plates. Given one potential cause is the absorption of lipophilic molecules during culture by PDMS, the PS devices were also assayed using phenol-red-free media with charcoal-stripped serum. The fraction of cells ALDH1^{HI} increased using the stripped medium, supporting this concept, but not to the full extent of the PDMS condition.

Cell morphology analysis

As an additional means to assess the impact of Tape material on cell culture, cell morphology was analyzed. Fig 3E provides visual evidence that cell morphology is consistent within cell types and across device types. The image data is further quantified in Fig 3F. In this experiment, if Tape material significantly impacts cell size / adhesion, Tape-containing device (PS-Milled, PS-Tape, and PS-Petri) would be expected to show similar significant differences from 96-Well Plate controls and would likely compare unfavorably to the microdevice gold-standard of PDMS. This was not the case. In most cases, the Tape-containing devices were not significantly different from the 96-Well Plate controls. In the case where differences were observed (RPMI cells), all differences were small (< 4% max deviation from group mean) and PS-Tape was more similar to 96-Well Plate than the microdevice gold standard of PDMS. Likewise, in the case of MDA-MB-231 cells, the PDMS control was different from all other device types, supporting results seen in Fig 3D, where Tape-containing devices produced results more similar to 96-Well plates than PDMS for MDA-MB-231 cells. Therefore, results do not suggest that Tape specifically influences cell morphology for any of the cell types relative to standard 96-well plates.

Compatibility with fluorescence microscopy

To assess compatibility of the Tape material with fluorescence microscopy, we first quantified Tape fluorescence using a fluorospectrometer (Fig 4A). Results show that Tape is excited by UV light that results in fluorescence primarily between 390 and 500 nm but did not produce detectable fluorescence when excited with white light (460–650 nm). We then assessed the intensity of this Tape fluorescence relative to cell staining in microscopy images (Fig 4B). When excited at 390 nm, Tape fluorescence was visible outside the culture well where Tape exists but was generally less intense than the nuclei and did not impact imaging inside the well where there was no Tape. When excited at 648 nm, Tape fluorescence was minimal compared to antibody staining, supporting spectrometry results. An additional demonstration using different cells, stains, and microscope is provided in Fig S4 of the SI. It should also be noted that no alterations to standard protocols were necessary for any of the staining protocols and no adsorption/absorption of fluorescent antibody was observed on the Tape at the culture well boundary.

MALDI-ToF MS analysis of fluid from devices

Polymers, such as PDMS, can potentially leach uncrosslinked components or compounds into culture media [28]; therefore, we used mass spectrometry to examine whether components of Tape can be detected in aqueous samples or if washing of PS-Tape devices could reduce levels of such compounds. The composition of Tape was proprietary, therefore comparative analysis was performed. Ethanol was used to dissolve tape components to generate a positive control spectrum while matrix only was used as a negative control. The roughly Gaussian distribution of peaks in the positive control that is characteristic of polymers could be readily observed (Fig S1). However, water samples incubated with Tape after different numbers of washes (X, Y, Z) were indistinguishable from the matrix-only negative control.

Bubble entrapment

A common challenge of microscale culture assays is the entrapment of bubbles given they can restrict or stop fluid flow in channels, affect culture viability, or compromise imaging. Bubble formation in PS-Tape channels was examined and is summarized in Fig 5. Significant bubble formation in enclosed microchannels was observed for devices placed on tissue culture plastic (TCP), but not on untreated glass or in the open-well devices used in Fig 3 & 4. However, bubble formation on TCP could be avoided if the device was heated to promote outgassing, prior to filling with culture media.

Ultra-rapid prototyping

To demonstrate use of tape-based razor-printing for ultra-rapid prototyping of common culture assays, 3 devices that were designed, constructed, and imaged in a total of 3 hours (Fig 6). Devices include (i) a basic straight-channel with an input port and output, (ii) a two-chamber co-culture device that utilizes two channels connected by a narrow diffusion region to restrict cross flow, and (iii) a microfluidic version of a transwell with a polyester track-etch membrane separating two culture regions. The transwell example specifically illustrates how the tape can be used to facilitate insertion and sealing of membranes or potentially other materials between device layers. [11,22]

Tape-based integration of sheet materials

Tape-based razor-printing enables integration and patterning of other biocompatible sheet materials within devices to enable unique device functionality for cell-based applications. To demonstrate this capability, electrospun collagen was laminated with biomedical adhesive tape, cut, and placed in the culture regions of the open-well co-culture device (Fig 7). The use of two different electrospun matrices demonstrates the ability to pattern electrospun biomaterials of different properties into a single microscale device, something that is challenging to do directly using electrospinning techniques. [37–40]

DISCUSSION

Suitability of Tape for cell-based microscale device fabrication

Tape-based razor-printing has gained momentum as a microscale device fabrication method. [1–11,18,19,21,41] However, a particular choice of biocompatible adhesive tape has not been identified or embraced as a legitimate option for cell-based applications. Without such an option, future application of this powerful method for cell-based applications will be limited. Thus, in efforts to advance the repertoire of biocompatible tapes, we characterized use of ARcare 90106 biomedical adhesive tape (Tape) with polystyrene (PS) sheets for building layered razor-printed devices. This tape was chosen given that it has shown promise in terms of biocompatibility in multiple applications [22,42–45]; however, as with other biomedical-grade adhesive tapes, the effects of the material in devices was not validated against gold-standard approaches or characterized with respect to other important material traits for microscale culture device fabrication. Thus, we first sought to characterize the tape-based devices with respect to cytotoxicity/viability/morphology, absorption/adsorption of small lipophilic molecules, bubble nucleation/outgassing, and prototyping/fabrication time and cost.

Cell viability characterization of Tape was performed by comparing monoculture in 4 different open microdevice constructions (Fig 3) with that of monoculture in a 96-well plate using cell viability of 3 different well-studied cell lines (LNCaP, MCF-7, and RPMI 8226). These cell lines were chosen both for their wide use in cancer studies (prostate, breast, and multiple myeloma respectively) and their representation of adherent and nonadherent cell types. Tape-containing devices had cell viabilities equivalent to PDMS devices and well-plates, regardless of cell type (Fig 3A).

Morphological analysis did not provide evidence to suggest that the Tape significantly influences cell morphology (Fig 4E & 4F). Although, this result suggests that the Tape does not significantly influence the cell cultures tested, negative results are not conclusive. Thus, additional evaluation is still recommended for each new biological application. Morphological results did, however, suggest that Tape-containing devices may produce results more similar to 96-well plates than the microdevice gold-standard of PDMS for MDA-MB-231 cells.

The encouraging cell viability and morphology results provided a first direct comparison of tape-based razor-printed devices with analogous microscale and macroscale culture devices

and did so using a range of cell types, giving us confidence to move forward with additional characterization.

Given the importance of microscopy in cell biology, it was important to characterize the compatibility of Tape-based devices with standard cell staining and imaging techniques. Using fluorospectrometry, we found that exciting Tape with UV light causes fluorescence primarily in blue wavelengths (390–500 nm) while wavelengths > 460 nm did not cause appreciable fluorescence. During fluorescence microscopy, we found that the Tape-containing devices required no alteration of standard staining and imaging protocols for DAPI, EdU, Calcein, EtHD, AldeRed, and fluorescence antibody staining (Fig 3 & 4). However, if one must image directly through Tape, background fluorescence in the blue (390–500 nm) and potentially green (500–570 nm) wavelengths should be considered when cell staining intensities are low.

Given the tape is moderately hydrophobic (H_2O contact angle ~76°), we examined the extent to which the material sequesters hydrophobic small molecules (e.g., cell signaling molecules such as estrogens) from aqueous solutions given that PDMS, another hydrophobic polymeric material used extensively in cell-based applications, is known to do so. [28,35] Qualitatively, differences could be observed in the rhodamine absorption/adsorption characteristics of PDMS and PS-Tape laminate via imaging (Fig 3B), suggesting rhodamine adsorption is noticeable but penetration into the Tape is limited. Upon more quantitative examination, measurements of the EC50 of estrogen (E2) response in reporter cell lines did not show significant differences (Fig 3C) and suggest that lipophilic adsorption/absorption is not a limiting factor for cell-based studies. Indeed, subsequent estrogen sensitivity experiments with two additional cell lines (MDA-MB-468 and MDA-MB-231) shown in Fig 3D support this as well. The PS-Tape devices produced results more similar to 96-well plates than PDMS devices in terms of cell differentiation (AldeRed ALDH assay) [46] with and without estrogen. However, validation or dose-response characterization for specific applications involving small hydrophobic molecules is warranted.

Mass-spectrometry was also performed to detect the presence of polymers that might leach into the aqueous media and influence culture in other, less-defined ways (Fig S1). Although polymer could be readily detected in positive controls of ethanol-dissolved tape components, aqueous samples incubated with the tape could not be readily distinguished from the matrix-only negative controls. Although this does not eliminate the possibility of tape components leaching into cell culture media, it further supports the notion of this tape as a promising material for cell culture applications. More extensive mass-spectrometry characterization is difficult at this point given the unknown chemical nature of the proprietary material.

A common challenge of microscale culture assays is the entrapment of bubbles. Typically, solubility of gas in solution or polymers goes down as temperature goes up, promoting bubble nucleation and outgassing upon incubation for cell culture. Whereas bubble formation is generally not a worry in open device designs where potentially super-saturated levels of gas in solution can readily equilibrate with surroundings or escape, bubbles trapped in closed designs can restrict or stop fluid flow, affect cell viability, or impede microscopy. Interestingly, significant bubble formation was not observed when PS-Tape microchannels

were placed on untreated glass (Corning, 2947-75×25, contact angle ~40°) but was observed when placed on tissue culture plastic (TCP) (Corning, Falcon, 353003, contact angle ~40°). We explored this further using different treatments to influence tape hydrophobicity, moisture content, and outgassing. We found that heating the devices placed on TCP to 60°C for 2hrs prior to filling channels with media was sufficient to prevent bubble formation for at least 48 hours in an incubator at 37°C. Furthermore, we confirmed that the heat treatment did not affect cell viability using cultures of MCF-7 breast cancer cells compared to previous culture experiments in open devices (~97%, Fig S2). Heat treatment parameters have not been optimized; however, temperatures can likely be reduced but might slow purging of the gas. Thus, outgassing and the type of substrate appeared to be the primary influences on bubble formation and heat treatment of the device is recommended prior to filling to address bubble formation if needed.

Razor-printing of PS-Tape devices also compared favorably with other microscale device fabrication methods. For example, we found that razor-printing of PS-Tape laminate devices was rapid (~1 hr prototyping time), required a relatively low initial equipment investment (~ $1200), and had a low per device cost ($0.05 - prototype, $0.05 - subsequent per device cost) (Tab 1). However, the resolution is generally lower than other methods such as printed mask soft-lithography (~100 μm vs 30 μm XY, Tab 1). Likewise, whereas soft-lithography can mold multiple device layers of nearly any thickness at once, multi-layer razor-printed devices typically require additional assembly and options of layer thicknesses are limited by Tape and material dimensions. As with other device fabrication approaches, razor-printed devices can be arrayed into customized layouts for interfacing with standard laboratory automation (Fig S5) such as plate-readers and pipette automation. Lastly, the simplicity of razor-printing can be complemented with the simplicity, flexibility, and accessibility of open microscale device designs [26,27] to create an ultra-rapid and simple platform for broader adoption.

Taken together, the above experiments provided strong evidence that ARCare 90106 tape is a legitimate material option for enabling tape-based razor-printing of microscale devices for cell-culture applications. This is important given that, previously, tape-based razor printing had been acknowledged for its efficiency and flexibility but had not yet been significantly characterized or used as a method for developing and performing cell-based assays. However, as with any new material, validation is still recommended for each new biological application.

Strengths and enabling capabilities of biocompatible tape-based razor-printing

Given the promising validation data, we sought to illustrate the major capabilities that a biocompatible tape enables for cell-based applications.

Biocompatible tape-based razor-printing enables ultra-rapid prototyping of cell culture devices. This is demonstrated in Fig 6, which shows three different embodiments of microscale culture assays (simple microchannel, microchannel co-culture device with connecting diffusion channel, and micro-transwell device with integrated porous membrane) that were conceptualized, designed in software, printed, constructed, and imaged in a total of 3 hrs.

The tape-based fabrication can be leveraged to rapidly integrate materials that are typically hard to bond or provide additional functionality. For example, the devices of Fig 6 show bonding of PS to glass, two materials that are typically quite challenging to bond strongly. This is particularly advantageous for microscopy applications, allowing integration of coverslip glass with optically transparent and smooth PS sheets (vs rough micromilled PS). Device (iii) of Fig 6 also demonstrates the ability to include materials such as membranes for added functionality.

The ability to integrate disparate materials provides significant opportunity for developing new applications. Fig 7 illustrates integration of contrasting electrospun biomaterials into the same device. Integration of tape-based razor-printing and electrospun materials is innovative in multiple respects. For the past 20 years, electrospinning technique has been widely used in tissue engineering applications to generate of both natural and synthetic biomimetic fibers and provide control over key parameters that modulate cell adhesion, migration, and differentiation (e.g., fiber interconnectivity, porosity, diameter, and orientation). However, the use of electrospun fibers in microscale models has been limited by challenges in precisely controlling the location of fiber deposition within the geometric constraints of devices. [39,40] The biocompatible double-sided adhesive tape provided structural support for razor-printing of the fragile electrospun sheets to enable patterning of highly disparate materials within a single microdevice, greatly expanding the potential applications of electrospun fibers for microscale applications.

Lastly, the approach is easy to adopt and can be readily applied to a broad range of new application settings. For example, the data of Fig 3D represents a culture experiment in which complete novices to razor-printing were able to learn to use the equipment, apply it, and successfully recapitulate results observed in conventional TCP 96 well plates in ~ 1 week. Furthermore, the devices can, in many ways, be treated like stickers, enabling application of devices to new substrates (e.g., skin and plants) and different contexts (e.g., the bottom of a well in a 24-well plate), significantly expanding the range of substrates for applying biocompatible microscale devices.

We envision these strengths and capabilities will expand use of microscale technology not only for advanced studies of biology and disease, but also in other important areas, such as laboratories in undergraduate institutions, high schools, and resource-constrained settings.

CONCLUSION

The recognized potential of combining razor-printing and tape-based device fabrication have not yet been fully realized for cell-based applications due to lack of characterized and accepted biocompatible adhesive tapes. For this reason, we provided, to our knowledge, a first head-to-head cell-culture comparison of razor-printed devices containing biocompatible double-sided tape (ARCare 90106) with common microscale and macroscale alternatives. To strengthen these studies, a variety of different experiments were performed involving 8 different cell lines, each suggesting that the tape material is biocompatible and suited for cell-based studies. We then demonstrated that razor-printing of PS-Tape laminate devices enabled ultra-rapid and robust fabrication of custom sticker-like device designs (~ 1hr) with

minimal equipment investment ($1,200) and cost per prototype ($0.05). We believe the ability to easily and rapidly fabricate biocompatible devices, pattern different sheet-based materials within each device, and apply those devices like stickers to a wide range of potential substrates and contexts will open a wide range of new cell-based applications in microscale assay development.

Supplementary Material

Refer to Web version on PubMed Central for supplementary material.

Acknowledgments

We would like to thank the following individuals and organizations for important contributions and financial support. Theodorus de Groot and Patrick Ingram for editing and reviewing this manuscript. Support for DJB, JWW, YAG, & LES - NIH-NCI 4R01 CA155192. Support for LES - The National Human Genome Research Institute through the Genomic Science Training Program 5T32HG002760. Support for KPR, AMR, & MD - NIH-NCI 1K01 CA188167 and NSF-CREST HRD-1345156 at UPR-Mayaguez. Support for MMM - NIH T32 ES007015-39 and EPA grant number 83573701. Prof. Shigeki Miyamoto - Generously donated RPMI 8226 cells. Prof. Elaine Alarid - Generously donated MCF-7 MVLN cells. Adhesives Research, Inc. generously donated some of the ARCare 90106 tape for the studies. Dr. Jorge Almodovar, from University of Puerto Rico-Mayaguez, generously donated clinical grade collagen type I (Integra Life Sciences) and provided access to electrospinning instrumentation. David J. Beebe holds equity in Bellbrook Labs LLC, Tasso Inc., Stacks to the Future LLC, Lynx Biosciences LLC, Onexion Biosystems LLC and Salus Discovery LLC.

BIBLIOGRAPHY

1. Martínez-López JI, Mojica M, Rodríguez CA, Siller HR. Xurography as a Rapid Fabrication Alternative for Point-of-Care Devices: Assessment of Passive Micromixers. Sensors. 2016; 16
2. Cosson S, Aeberli LG, Brandenberg N, Lutolf MP. Ultra-rapid prototyping of flexible, multi-layered microfluidic devices via razor writing. Lab Chip. 2014; 15:72–76.
3. de Santana PP, de Oliveira IMF, Piccin E. Evaluation of using xurography as a new technique for the fabrication of disposable gold electrodes with highly reproducible areas. Electrochem commun. 2012; 16:96–99.
4. Greer J, Sundberg SO, Wittwer CT, Gale BK. Comparison of glass etching to xurography prototyping of microfluidic channels for DNA melting analysis. J Micromech Microeng. 2007; 17:2407–2413.
5. Renaud L, Selloum D, Tingry S. Xurography for 2D and multi-level glucose/O2 microfluidic biofuel cell. Microfluid Nanofluidics. 2015; 18:1407–1416.
6. Yuen PK, DeRosa ME. Flexible microfluidic devices with three-dimensional interconnected microporous walls for gas and liquid applications. Lab Chip. 2011; 11:3249–3255. [PubMed: 21833418]
7. Pessoa de Santana P, et al. Fabrication of glass microchannels by xurography for electrophoresis applications. Analyst. 2013; 138:1660. [PubMed: 23392529]
8. Zhang J, et al. A Disposable Microfluidic Virus Concentration Device Based on Evaporation and Interfacial Tension. Diagnostics. 2013; 3:155–169. [PubMed: 26617991]
9. Focke M, et al. Lab-on-a-Foil: microfluidics on thin and flexible films. Lab Chip. 2010; 10:1365–1386. [PubMed: 20369211]
10. Pinto E, et al. A Rapid and Low-Cost Nonlithographic Method to Fabricate Biomedical Microdevices for Blood Flow Analysis. Micromachines. 2014; 6:121–135.
11. Goral VN, Zhou C, Lai F, Yuen PK. A continuous perfusion microplate for cell culture. Lab Chip. 2013; 13:1039–1043. [PubMed: 23344077]
12. Khademhosseini A, Langer R, Borenstein J, Vacanti JP. Microscale technologies for tissue engineering and biology. Proceedings of the National Academy of Sciences. 2006; 103:2480–2487.

13. Guckenberger DJ, de Groot TE, Wan AMD, Beebe DJ, Young EWK. Micromilling: a method for ultra-rapid prototyping of plastic microfluidic devices. Lab Chip. 2015; 15:2364–2378. [PubMed: 25906246]
14. Ho CMB, Ng SH, Li KHH, Yoon YJ. 3D printed microfluidics for biological applications. Lab Chip. 2015; 15:3627–3637. [PubMed: 26237523]
15. Amin R, et al. 3D-printed microfluidic devices. Biofabrication. 2016; 8:022001. [PubMed: 27321137]
16. Xia Y, Whitesides GM. Soft Lithography. Angew Chem Int Ed. 1998; 37:550–575.
17. Duffy DC, McDonald JC, Schueller OJ, Whitesides GM. Rapid Prototyping of Microfluidic Systems in Poly(dimethylsiloxane). Anal Chem. 1998; 70:4974–4984. [PubMed: 21644679]
18. Bartholomeusz DA, Boutte RW, Andrade JD. Xurography: rapid prototyping of microstructures using a cutting plotter. J Microelectromech Syst. 2005; 14:1364–1374.
19. Kim J, Surapaneni R, Gale BK. Rapid prototyping of microfluidic systems using a PDMS/polymer tape composite. Lab Chip. 2009; 9:1290–1293. [PubMed: 19370251]
20. Yuen PK, Goral VN. Low-cost rapid prototyping of flexible microfluidic devices using a desktop digital craft cutter. Lab Chip. 2010; 10:384–387. [PubMed: 20091012]
21. Yuen PK, Goral VN. Low-cost rapid prototyping of flexible microfluidic devices using a desktop digital craft cutter. Lab Chip. 2010; 10:384–387. [PubMed: 20091012]
22. Goral VN, Tran E, Yuen PK. A pump-free membrane-controlled perfusion microfluidic platform. Biomicrofluidics. 2015; 9:054103. [PubMed: 26392835]
23. Neuville A, et al. Xurography for microfluidics on a reactive solid. Lab Chip. 2017; 17:293–303. [PubMed: 27934975]
24. Yuen PK, Goral VN. Low-cost rapid prototyping of flexible microfluidic devices using a desktop digital craft cutter. Lab Chip. 2010; 10:384–387. [PubMed: 20091012]
25. Berthier, J., Brakke, KA., Berthier, E. Open Microfluidics. John Wiley & Sons; 2016.
26. Casavant BP, et al. Suspended microfluidics. Proc Natl Acad Sci U S A. 2013; 110:10111–10116. [PubMed: 23729815]
27. Sackmann EK, Fulton AL, Beebe DJ. The present and future role of microfluidics in biomedical research. Nature. 2014; 507:181–189. [PubMed: 24622198]
28. Regehr KJ, et al. Biological implications of polydimethylsiloxane-based microfluidic cell culture. Lab Chip. 2009; 9:2132–2139. [PubMed: 19606288]
29. Kuperwasser C, et al. Reconstruction of functionally normal and malignant human breast tissues in mice. Proc Natl Acad Sci U S A. 2004; 101:4966–4971. [PubMed: 15051869]
30. Warrick, Erwin, J. [Accessed: 14th January 2016] JEX. Available at: https://github.com/jaywarrick/JEX
31. Demirpence E, Duchesne MJ, Badia E, Gagne D, Pons M. MVLN Cells: A bioluminescent MCF-7-derived cell line to study the modulation of estrogenic activity. J Steroid Biochem Mol Biol. 1993; 46:355–364. [PubMed: 9831484]
32. Warrick JW, Timm A, Swick A, Yin J. Tools for Single-Cell Kinetic Analysis of Virus-Host Interactions. PLoS One. 2016; 11:e0145081. [PubMed: 26752057]
33. Schneider CA, Rasband WS, Eliceiri KW. NIH Image to ImageJ: 25 years of image analysis. Nat Methods. 2012; 9:671–675. [PubMed: 22930834]
34. Rueden CT, et al. ImageJ2: ImageJ for the next generation of scientific image data. BMC Bioinformatics. 2017; 18:529. [PubMed: 29187165]
35. Toepke MW, Beebe DJ. PDMS absorption of small molecules and consequences in microfluidic applications. Lab Chip. 2006; 6:1484–1486. [PubMed: 17203151]
36. Bonefeld-Jørgensen EC, Long M, Hofmeister MV, Vinggaard AM. Endocrine-Disrupting Potential of Bisphenol A, Bisphenol A Dimethacrylate, 4-n-Nonylphenol, and 4-n-Octylphenol in Vitro: New Data and a Brief Review. Environ Health Perspect. 2007; 115:69–76. [PubMed: 18174953]
37. Carlberg B, Wang T, Liu J. Direct photolithographic patterning of electrospun films for defined nanofibrillar microarchitectures. Langmuir. 2010; 26:2235–2239. [PubMed: 20092342]
38. Teo WE, Ramakrishna S. A review on electrospinning design and nanofibre assemblies. Nanotechnology. 2006; 17:R89–R106. [PubMed: 19661572]

39. Kameoka J, et al. A scanning tip electrospinning source for deposition of oriented nanofibres. Nanotechnology. 2003; 14:1124.

40. Ladd, MR., Hill, TK., Yoo, JJ., Lee, SJ. Nanofibers-Production, Properties and Functional Applications. InTech; 2011. Electrospun nanofibers in tissue engineering.

41. Yuen PK, Goral VN. Low-cost rapid prototyping of flexible microfluidic devices using a desktop digital craft cutter. Lab Chip. 2010; 10:384–387. [PubMed: 20091012]

42. Nath P, et al. Polymerase chain reaction compatibility of adhesive transfer tape based microfluidic platforms. Microsyst Technol. 2013; 20:1187–1193.

43. Harkness T, et al. High-content imaging with micropatterned multiwell plates reveals influence of cell geometry and cytoskeleton on chromatin dynamics. Biotechnol J. 2015; 10:1555–1567. [PubMed: 26097126]

44. Kloth K, Niessner R, Seidel M. Development of an open stand-alone platform for regenerable automated microarrays. Biosens Bioelectron. 2009; 24:2106–2112. [PubMed: 19110413]

45. Sauceda-Friebe JC, et al. Regenerable immuno-biochip for screening ochratoxin A in green coffee extract using an automated microarray chip reader with chemiluminescence detection. Anal Chim Acta. 2011; 689:234–242. [PubMed: 21397079]

46. Minn I, et al. A red-shifted fluorescent substrate for aldehyde dehydrogenase. Nat Commun. 2014; 5:3662. [PubMed: 24759454]

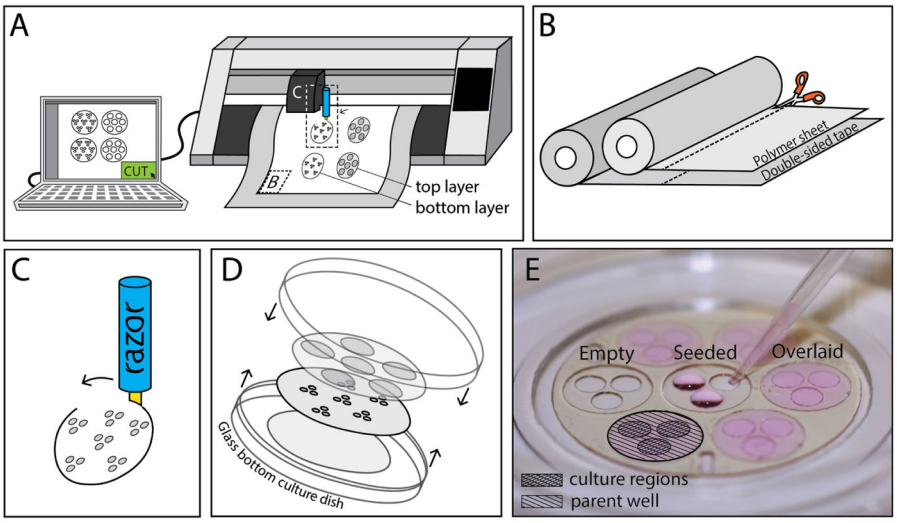

Figure 1. Tape-based razor-printing fabrication of microscale sticker devices

(A) Automated cutting plotter based on printer technology allows razor-printing (xurography) for precisely cutting shapes from sheets of material. (B) Example of a cuttable laminate formed by marrying a polymer sheet (e.g., PS) and a sheet of double sided adhesive tape. (C) The razor of the cutting plotter cuts through the laminate to create device components. (D) Cut components are layered to form devices and 3D structures that can be applied like a sticker to a wide variety of substrates. (E) Example of a razor-printed co-culture sticker device fabricated using PS-Tape laminate, cell seeding procedure, and nomenclature of different device regions.

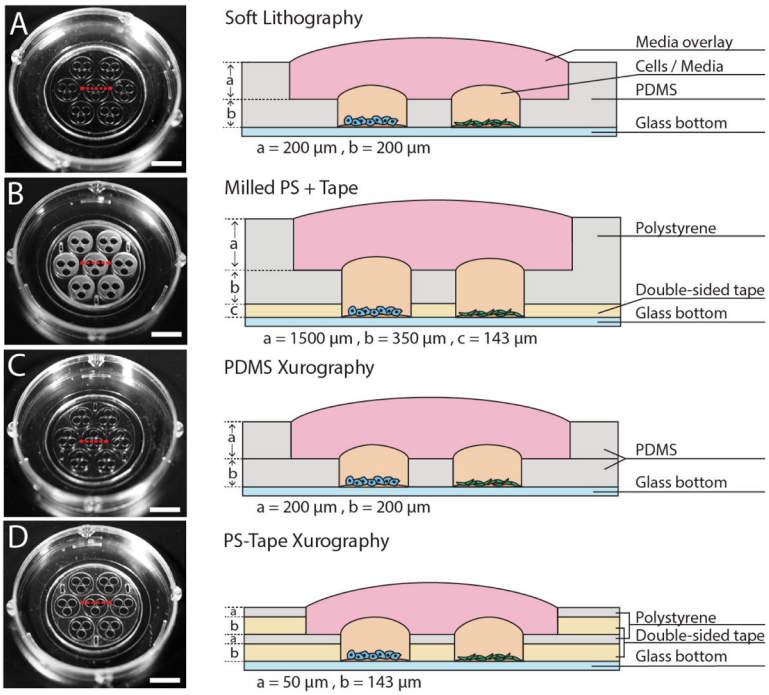

Figure 2. Nested co-culture device design and construction

Photos of devices fabricated with four techniques and cross-sectional schematic of the device components. Manufacturer thicknesses of PS sheeting and Tape are 0.05 mm and 0.143 mm, respectively. (A) Device constructed from PDMS using soft lithography. (B) Device constructed using micromilled PS and razor-printed double-sided biomedical adhesive tape. (C) Razor-printed PS-Tape laminate device. (D) Razor-printed PDMS device. (solid white lines) 10 mm scale bar. (dashed red lines) region of the cross-section schematic.

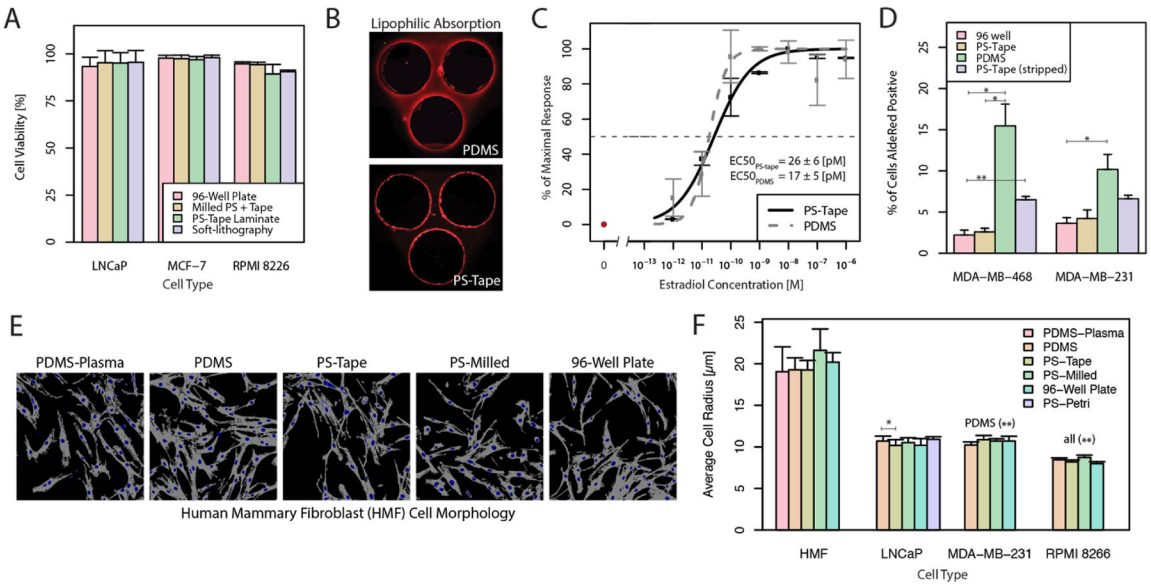

Figure 3. Cell viability, morphology, and device absorption of lipophilic molecules

(A) Cell viability at 24 hrs by cell type (MCF-7, LNCaP, or RPMI 8226) and device construction (96-well plate, Milled PS + tape, PS-Tape laminate, or PDMS soft-lithography) in 2D culture. (B) Images of nile red adsorbed/absorbed to/in a PS-Tape and PDMS device. (C) Graph of estradiol (E2) dose-response curves for MVLN ERE luciferase reporter cell line in PS-Tape and PDMS co-culture devices. (D) MDA-MB-468 and MDA-MB-231 were mono-cultured in 96-well plates and co-culture devices made of PDMS or razor-cut PS-Tape using low serum DMEM culture medium or no-phenol DMEM with charcoal stripped serum (stripped) for 96 hrs. AldeRed was used to quantify the % of total cells with high levels of the stem cell marker ALDH1 (ALDH1 ^{HI}). (E) Cell morphology of HMF cells cultured in different device types. Brightfield and nuclear stained images are thresholded and overlaid to show regions of cytoplasm (gray) and nuclei (blue) to aid comparison. Images of other cells types (LNCaP, MDA-MB-231, and RPMI 8226) are contained in Fig S3. PDMS-Plasma refers to a PDMS device in which the glass culture substrate was pretreated via oxygen plasma treatment. (F) Plot of average equivalent cell radius for each cell type in each culture device type ($^{*}\leq 0.05$, $^{**}\leq 0.01$, t-test, two-tailed, Bonferroni correction, error-bars indicate std. dev.).

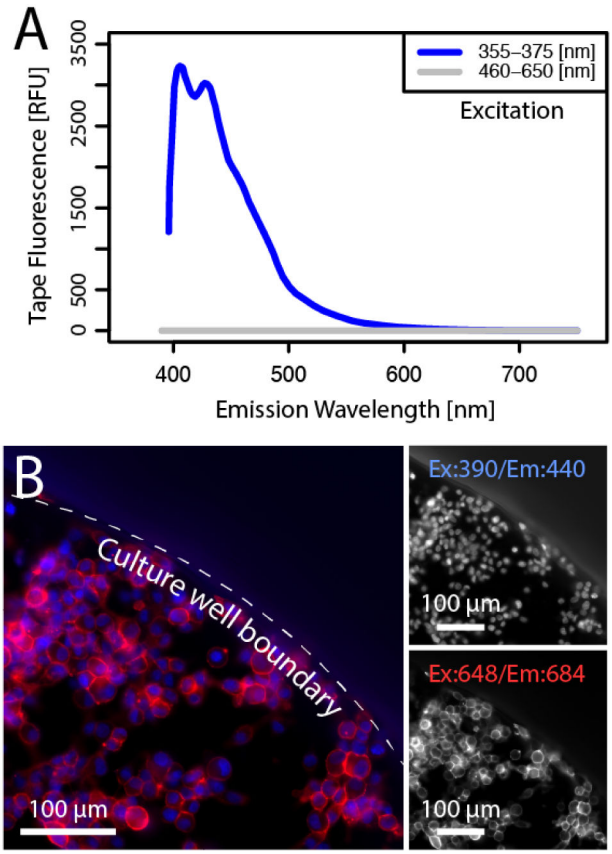

Figure 4. Analysis of tape fluorescence and demonstration of immunofluorescence staining

(A) Tape fluorescence measured using a Nanodrop 3300 fluorospectrometer (Thermo Scientific) using the UV excitation mode (355–375 nm) or white light excitation mode (460–650 nm). (B) LNCaP cells were stained using DAPI nuclear stain (top-right) and anti-EpCAM (epithelial cell adhesion molecule) fluorescent antibody (bottom-right). (left) False colored and magnified overlay of nuclear labeling (blue) and expression of the cell membrane protein EpCAM (red). Grayscale images have an intensity range of 0–255 units. Tape fluorescence outside the culture well was ~22 units for 390/440 nm and ~1 unit for 648/684 nm.

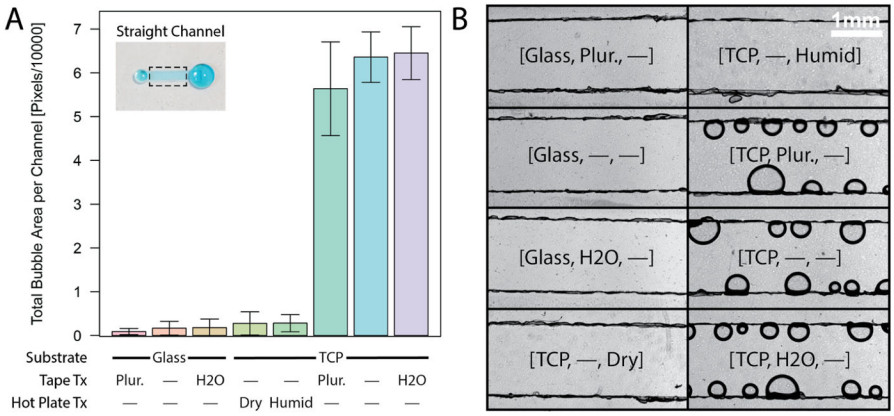

Figure 5. Bubble Formation in Tape Channels

Microchannels were cut into Tape and overlaid with a razor-printed PS port layer and placed onto either untreated glass (Glass) or tissue culture polystyrene (TCP) and filled with culture media containing 10% fetal bovine serum. Tape treatment (Tape Tx) conditions consisted of sonicating the tape layer alone for 30 min in either a 1% Pluronic F-127 solution in PBS (Plur.) or DI H_2O (H2O), while hot plate treatment (Hot Plate Tx) conditions consisted of incubating the assembled channel at 60°C for 2hrs in either a dry Petri dish (Dry) or dish containing 1 mL DI H_2O and sealed with parafilm (Humid). (A) Quantification of spontaneous bubble formation after 2 days incubation at 37°C. Each of the Glass and Hot Plate-treated TCP conditions were significantly different than the non-Hot Plate-treated TCP conditions ($p < 0.001$), and the [TCP,Plur.,—] condition was significantly different than both the [TCP,—,—] and [TCP, H2O, —] conditions ($p < 0.05$). Significance not shown in figure for readability, and n = 10 technical replicates. (B) Brightfield microscopy images (2X) of the quantified conditions in (A), using the notation [<Substrate>, <Tape Tx>, <Hot Plate Tx>]. No treatment is denoted with an em dash (—).

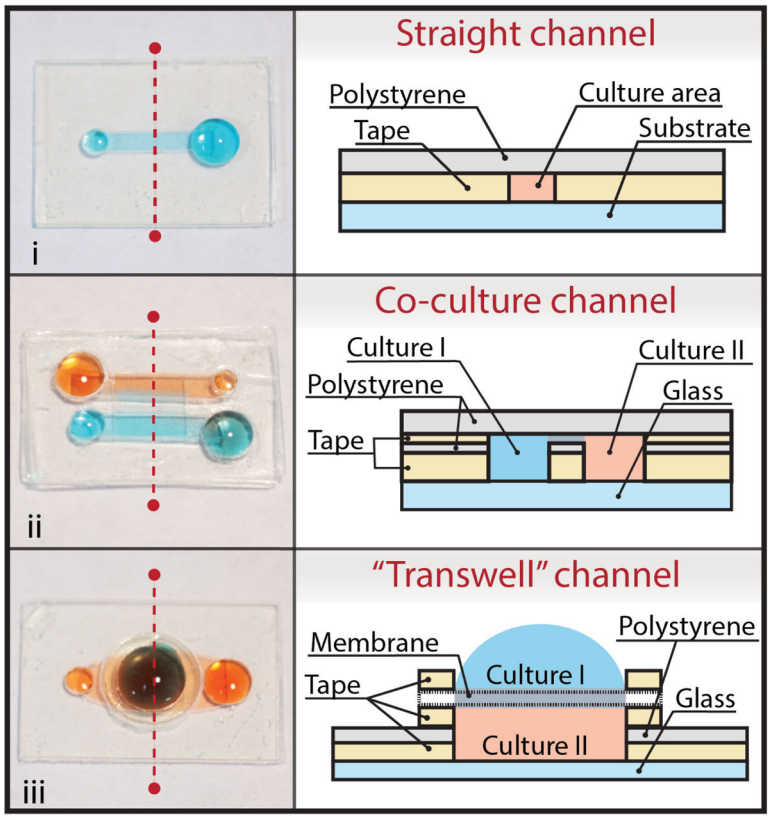

Figure 6. Rapid prototyping of 3 different cell culture assay designs

Images and schematics illustrate device construction. The schematics to the right of the images depict cross-section views of each device at the red dashed line.

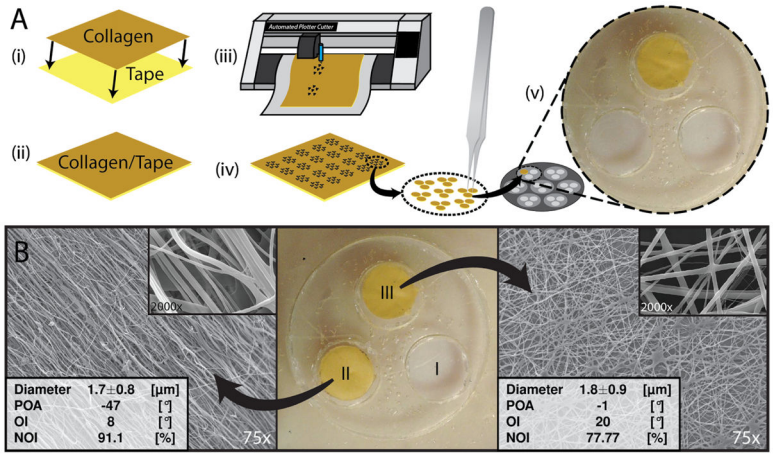

Figure 7. Razor-printing and patterning of electrospun collagen sheets

(A) Processing of electrospun collagen sheets for patterning via razor-printing. (i) Bonding of collagen sheet to ARcare 90106 exposed surface. (ii) Collagen/Tape sheet for use in automated plotter cutter. (iii) Automated cutting of the geometric pattern through collagen/Tape sheet. (iv) Collect pieces cut-out from collagen/Tape sheet and peel-off back layer for binding on TCP or glass surface (v). (B) Prototype of a PS microwell array containing adjacent microwells with 3 different culture surfaces: TCP (I), aligned collagen fibers (II) and randomly- oriented collagen fibers (III). POA = prevalent orientation angle and OI = orientation indices (a measure of angle variability) and NOI = normalized orientation index (0% or 100%=aligned, 50%=random).

Table 1

Comparison of device construction methods.

Characteristic	Unit	A. Soft lithography	B. Milled PS + Tape	C. PDMS Xurography	D. PS-Tape Xurography
XY-Resolution	[μm]	30±5[†]	150±50	100±30	100±30
Z-Resolution	[μm ± %]	>5±5	PS:>5±5, Tape:>25±10	>150±251[‡]	PS:>25±5, Tape:>25±10
Equip. Investment	[$]	13k	11k	2k	2k
Prototyping Time	[h]	48	4	3	1
Prototype Cost	[$]	200	1	0.5	0.05
Subsequent Device Cost	[$]	0.5	1	0.5	0.05

[†]Cost and resolutions based upon use of more affordable ink photomasks for prototypes as opposed to high-resolution chrome photomasks.

[‡]Cost and Z-resolution are based upon making PDMS sheets made without the aid of a spin coating machine, which would significantly increase equipment cost.